Chapter 5

MSR Breeder Fuels

The composition of MSR Breeder fuel

The uranium resources on Earth are plenty at the moment. May it happen that the reserves become too uneconomical to mine in the future, the use of thorium will be an alternative. Its natural abundance is about three times higher than for uranium [2].

The MSR has the capability of the breeding of uranium from thorium in a thermal spectrum, where neutron capture of ^{232}Th forms ^{233}Th, decaying rapidly to ^{233}Pa, which decays with a half-life of 27 days to ^{233}U, a fissile isotope. The reaction is depicted in Figure 5.1. Not only the best neutronic conditions facilitating this reaction, but also other thermal and physicochemical requirements have to be met. It has been proven that ^{7}LiF-BeF_2 is the most appropriate solvent for this fuel type. A small percentage of a fissile isotope, usually ^{235}U, is needed to start the neutron capture reaction. A typical fuel composition for the MSR is therefore a LiF-BeF_2-ThF_4-UF_4 mixture.

The contents of this Chapter were submitted as the papers Van der Meer, Konings and Oonk, "Thermodynamic assessment of the LiF-BeF_2-ThF_4-UF_4 system", J. Nucl. Mater. (in press) and Van der Meer and Konings, "Thermal and physical properties of molten fluorides for nuclear applications", J. Nucl. Mater. (accepted).

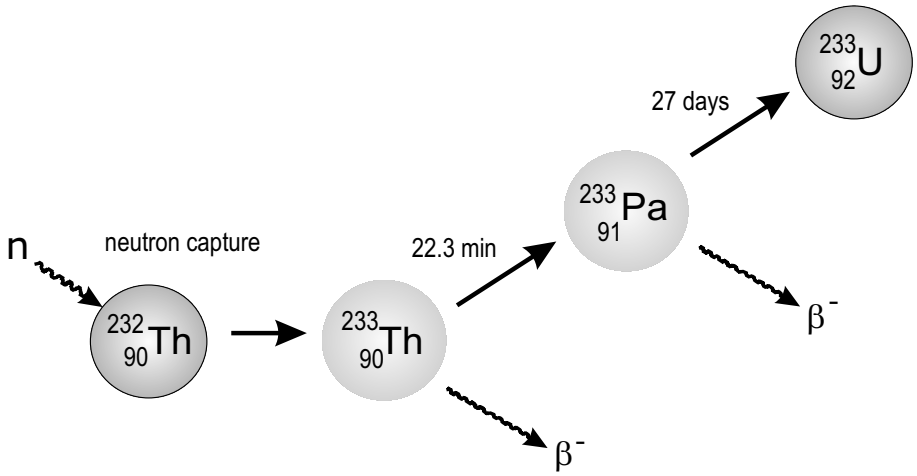

Figure 5.1: The thorium-uranium cycle. When ^{233}U decays, neutrons are released which can be captured by ^{232}Th to repeat the reaction.

Thermodynamic assessment of LiF-BeF_2-ThF_4-UF_4

The liquid phases of the LiF-BeF_2-ThF_4-UF_4 binary subsystems have been assessed using general polynomials, as was explained in Chapter 3 *Solvents*. By extrapolating the optimized Gibbs energy terms from the binaries, the ternary subsystems were calculated, which form the boundaries of the quaternary system.

For the compounds LiF, BeF_2, Li_2BeF_4, ThF_4 and UF_4, thermodynamic data were taken from an internal report [17]. This was not the case for the large number of intermediate compounds present in this system. Their Gibbs energy equations were obtained by optimization. All optimizations were done using the OptiSage module in the FactSage 5.3 software package [31]. It was assumed that, according to the Neumann-Kopp rule, the C_p could be added in weighted average of the pure compounds, while the enthalpy and entropy of formation needed to be assessed. Table 5.1 and lists these parameters, the literature data as well as the assessed values.

Table 5.1: $\Delta_f H^0$**(298.15 K),** S^0**(298.15 K) and** C_p **for the pure components and intermediate compounds containing fuels, as mentioned in this section**

Comp.	$\Delta_f H^0$(298.15 K) /kJ·mol^{-1}	S^0(298.15 K) /J·K^{-1}·mol^{-1}	a	b T /K	c T^{-2} /K^{-2}
ThF_4 (l)[a]	-2064.491	156.629	133.9		
UF_4 (l)[a]	-1914.658	115.400	174.74		
ThF_4 (cr)[a]	-2097.900	142.05	122.173	8.37E-3	-1.2550E+6
UF_4 (cr)[a]	-1914.200	151.7	114.5194	2.0555E-2	-4.1316E+5
Li_4UF_8 (cr)[b]	-4361.970	344.921	286.724	8.9841E-2	-2.6873E+6
$LiUF_5$ (cr)[b]	-2553.303	181.335	157.571	3.7877E-2	-9.8169E+5
LiU_4F_{17} (cr)[b]	-8367.599	577.206	501.129	9.95412E-2	-2.2212E+6
Li_3ThF_7 (cr)[b]	-4038.525	176.972	251.327	6.0335E-2	-2.9606E+6
$LiThF_5$ (cr)[b]	-2812.701	88.713	165.224	2.5692E-2	-1.8235E+6
$LiTh_2F_9$ (cr)[b]	-4929.261	229.395	287.397	3.4062E-2	-3.0785E+6
$LiTh_4F_{19}$ (cr)[b]	-9155.485	494.702	531.743	5.0802E-2	-5.5885E+6

[a] Data taken from an internal report [17].

[b] Obtained by assessment with the general polynomial model.

The binary subsystems of LiF-BeF$_2$-ThF$_4$-UF$_4$

Six binary subsystems are needed to build the four ternaries of which the quaternary LiF-BeF_2-ThF_4-UF_4 consists. LiF-BeF_2 was already described in Chapter 3 *Solvents*. As it was explained, the assessment demands the existence of a small miscibility gap near to the BeF_2 axis, in order to obtain an agreement between the enthalpy of fusion of BeF_2 and the experimental liquidus data.

LiF-ThF_4 and LiF-UF_4 are the most complex of the six diagrams containing a number of intermediate components: Li_3ThF_7, $LiThF_5$, $LiTh_2F_9$, $LiTh_4F_{17}$, respectively Li_4UF_8, $LiFUF_5$ and LiU_4F_{17}. The assessed diagrams of LiF-ThF_4 and LiF-UF_4 are shown in Figure 5.2, respectively 5.3.
BeF_2-ThF_4 and BeF_2-UF_4 are single eutectic systems with the eutectic point close to the BeF_2 axis. The assessed diagrams are shown in Figure 5.4, respectively 5.5. ThF_4 and UF_4 form a continuous solid solution series without a temperature minimum, but the experimental data, consisting of four points, are very limited. Figure 5.6 shows the ThF_4-UF_4 diagram. Data for the binaries can be found in Table 5.3.

Table 5.2: **Optimized excess Gibbs parameters of the liquid phase for the binaries of LiF-BeF_2-ThF_4-UF_4**

A, *B*	p	q	${}^{k}L_{A,B}$ /J·mol^{-1}	${}^{l}L_{A,B}$ /J·K^{-1}·mol^{-1}
UF_4-LiF	0	0	-75.252	-25.837
	0	1	-78694	38.406
ThF_4-LiF	0	0	-141298	102.50
	1	0	43130	-29.459
	0	1	-52637	38.821
BeF_2-LiF	0	0	-15580	-11.645
	1	0	71320	-63.487
	0	1	-71320	63.487
	1	1	-9612.0	0.000
	2	1	4806.0	0.000
	1	2	4806.0	0.000
UF_4-BeF_2	0	0	-33606	9.985
	1	0	-1630.0	27.447
	0	1	68012	-27.462
ThF_4-BeF_2	0	0	16749	-11.462
UF_4-ThF_4[a]	0	0	661.46	-1.4789

[a] ThF_4 and UF_4 form a solid solution.

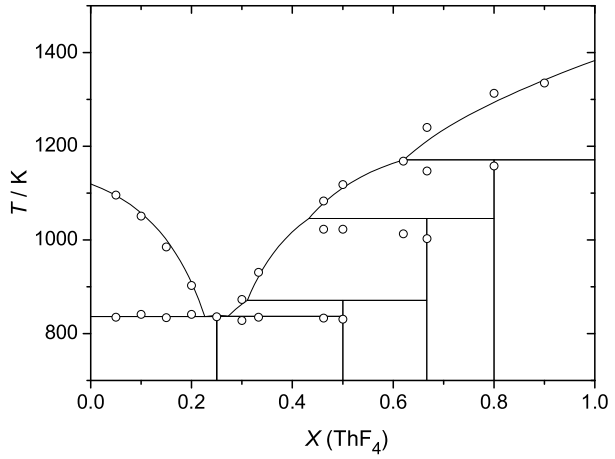

Figure 5.2: The assessed LiF-ThF$_4$ diagram; ∘ experimental data from Thoma *et al.* [77].

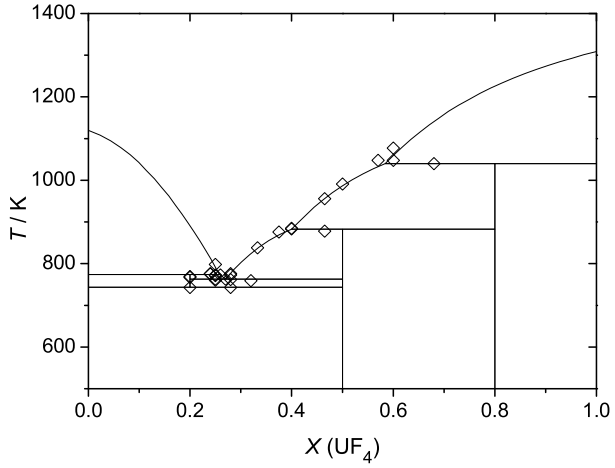

Figure 5.3: The assessed LiF-UF$_4$ diagram; ◊ experimental data by Thoma *et al.* [77].

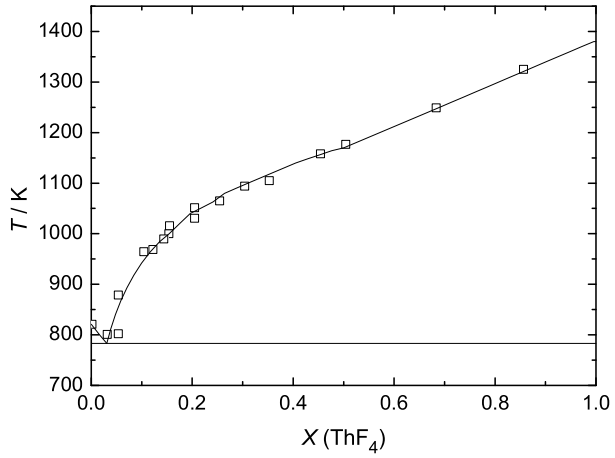

Figure 5.4: The assessed BeF_2-ThF_4 diagram; □ experimental data from Thoma *et al.* [78].

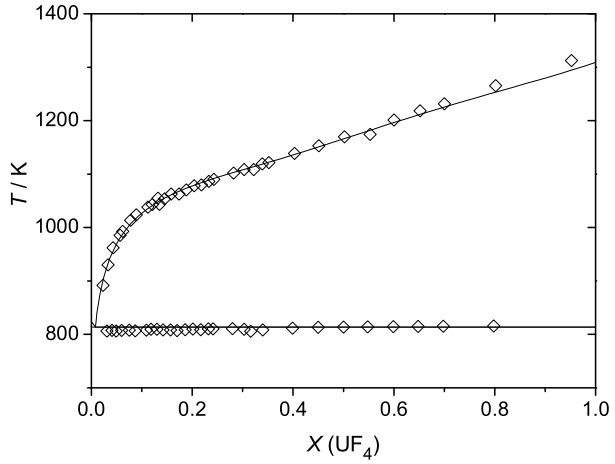

Figure 5.5: The assessed BeF_2-UF_4 diagram ◊ experimental data by Jones *et al.* [79].

Table 5.3: **Invariant equilibria in the binary subsystems of LiF-BeF$_2$-ThF$_4$-UF$_4$, calculated and *experimental (in italics)*[a]**

A–B	X_B	T/K	$X_{B,exp}$	T_{exp}/K	type invariant
LiF-UF$_4$[a]	0.200	742.8	*0.200*	*743*	lower stab. 4LiF·UF$_4$
	0.258	774.2	*0.26*	*773*	peritectic
	0.269	763.7	*0.27*	*763*	eutectic
	0.400	883.1	*0.40*	*883*	peritectic
	0.586	1040.0	*0.57*	*1048*	peritectic
LiF-ThF$_4$[b]	0.224	841.8	*0.23*	*841*	eutectic
	0.250	846.5	*0.25*	*846*	congr. m.p.
	0.283	840.0	*0.29*	*838*	eutectic
	0.302	855.7	*0.305*	*870*	peritectic
	0.428	1035.7	*0.42*	*1035*	peritectic
	0.603	1171.4	*0.62*	*1170*	peritectic
LiF-BeF$_2$[c]	0.330	728.6	*0.328*	732.0	eutectic
	0.333	728.7	*0.333*	*732.3*	congr. m.p.
	0.519	635.0	*0.531*	*636.7*	eutectic
	0.760	786.5	*not found*		begin RoD[f]
	0.871	811.9			max. RoD
	0.950	786.5			end RoD
BeF$_2$-UF$_4$[d]	0.008	813.6	*0.005*	*808*	eutectic
BeF$_2$-ThF$_4$[e]	0.023	794.8	*0.020*	*800*	eutectic

[a] Experimentally determined invariant points by Barton *et al.* [81].
[b] By Thoma *et al.* [77].
[c] By Romberger *et al.* [40].
[d] By Jones *et al.* [79].
[e] By Thoma *et al.* [78].
[f] Region of Demixing.

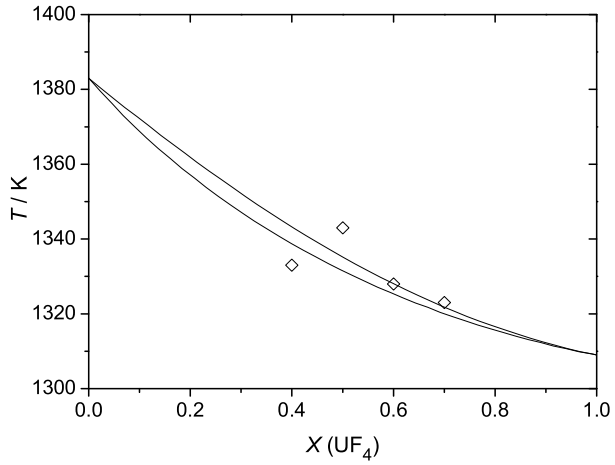

Figure 5.6: The assessed ThF_4-UF_4 diagram ◊ experimental data by Weaver *et al.* [80].

Calculation of higher order phase diagrams

The ternary phase diagrams were obtained by extrapolation of the binary interaction coefficients. The Kohler-Toop method was applied, which is suitable for chemically asymmetric systems. In the systems LiF-ThF_4-UF_4 and BeF_2-ThF_4-UF_4, the chemical asymmetric component is evidently LiF, respectively BeF_2. However, for LiF-BeF_2-ThF_4 and LiF-BeF_2-UF_4 discussion could arise how to treat the different components. In this case, LiF was selected as the asymmetric component, as will be explained in the paragraph *The asymmetric component in LiF-BeF_2-ThF_4*. An example of how three binaries are combined to a ternary diagram is seen in Figure 5.7, where the LiF-BeF_2-ThF_4 triangle is shown with the three binary subsystems forming its boundaries.

Figure 5.8 shows the calculated liquidus surface of LiF-BeF_2-ThF_4, LiF-BeF_2-UF_4, LiF-ThF_4-UF_4 and BeF_2-ThF_4-UF_4, such that they form a quaternary system. The figure can be considered as an open-folded tetrahedron with LiF-BeF_2-ThF_4 as the base and UF_4 at the apex.

LiF-BeF_2-ThF_4 contains a eutectic and a (quasi) peritectic point in the LiF rich part. Another eutectic (695.0 K) and a quasi peritectic (751.0 K) are found very near to the LiF-BeF_2 axis, which is indicated in Table 5.4. The assessed diagram of LiF-BeF_2-ThF_4 was published previously by us [82]. However, a

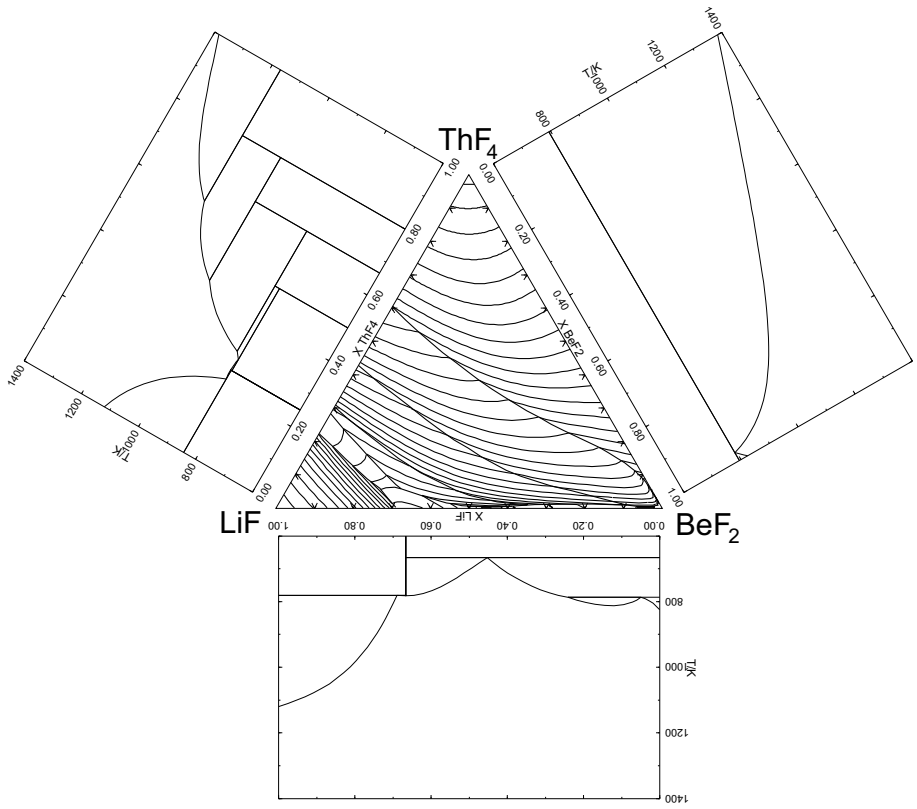

Figure 5.7: The projection of the liquidus surface of LiF-BeF$_2$-ThF$_4$. Isotherms with an interval of 25 K are shown. The three binary subsystems are along the sides.

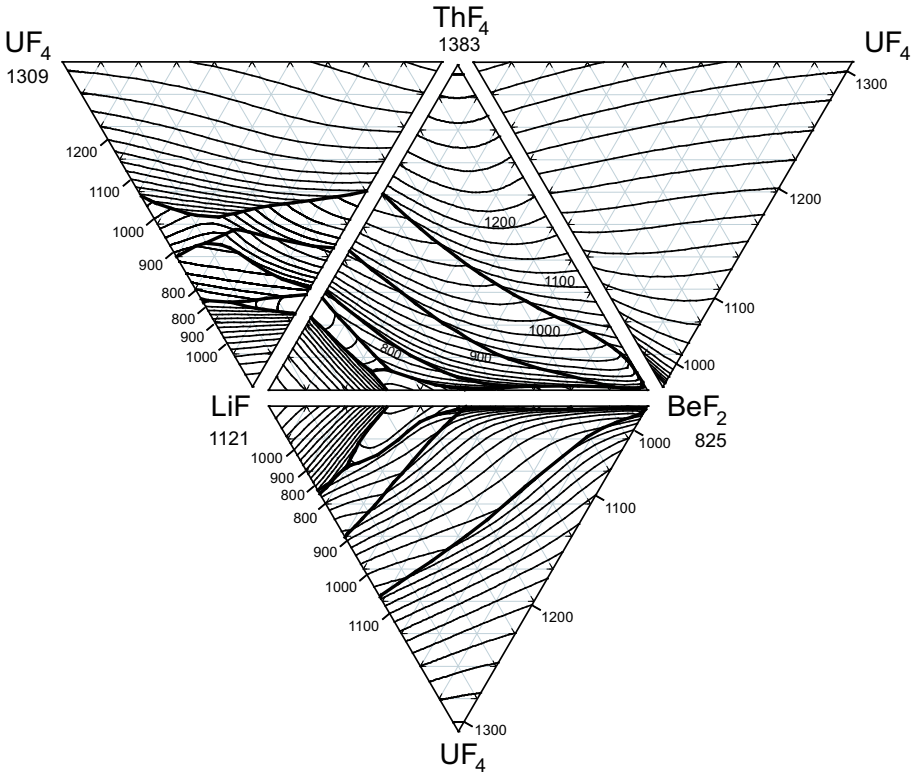

Figure 5.8: The calculated liquidus surface of LiF-BeF_2-ThF_4, LiF-BeF_2-UF_4, LiF-ThF_4-UF_4 and BeF_2-ThF_4-UF_4, combined to a quaternary system. Melting temperatures are labelled in K and isotherms with an interval of 25 K are shown.

modification of the diagram is shown here. The diagram we published first [82] was characterized by a significant ternary miscibility gap in the BeF_2 apex. A more thorough discussion can be found in the paragraph *The asymmetric component in LiF-BeF$_2$-ThF$_4$*.

LiF-BeF_2-UF_4 is analogous to the former system, but not similar, as LiF-UF_4 has one intermediate compound less than LiF-ThF_4. The point, at which LiF·4UF_4 decomposes, is very near to the LiF-UF_4 axis of the ternary. A eutectic can be found in the LiF rich region (712.9 K). Two other invariant points, a quasi peritectic (691.9 K) and eutectic (695.0 K), nearly touch the LiF-BeF_2 axis.

LiF-ThF_4-UF_4 contains three solid solution series: LiF·(Th,U)F_4, LiF·4(Th,U)F_4 and (Th,U)F_4. The solid-liquid phase diagram of ThF_4-UF_4 (Figure 5.6) shows evidence of weak deviations from ideal-mixing behavior. For that matter, the solid solutions were treated as ideal mixtures, putting all deviations from ideality in the liquid. One eutectic (760.2 K) and two quasi peritectic points (767.7 and 903.8 K)are present in this ternary. The invariant points of the three ternary systems mentioned above are described in Table 5.4.

The simplest of the four ternaries is BeF_2-ThF_4-UF_4, where the solid solution series between ThF_4 and UF_4 dominates. A ternary eutectic point does not exist, however, a eutectic line smoothly connects the two binary eutectics, which are almost at the BeF_2 apex.

Comparison ternary model and experimental data

Table 5.4 lists the invariant points of the systems LiF-BeF_2-ThF_4, LiF-BeF_2-UF_4 and LiF-ThF_4-UF_4, as found in the calculated diagrams and compares these to the experimentally derived values. It can be noticed that many calculated equilibria differ, not only in temperature, but also in composition, from the experimental ones. The composition of a ternary invariant point is sometimes not so straightforward as one would expect from studying the ternary diagram. When plotting binary cross-sections, the so-called pseudobinaries, far more complicated phase field relationships are revealed, which are not directly visible in the ternary.

Tables belonging to the papers [78, 79, 80], which were deposited at the Library of Congress in Washington D.C., contain all experimental data on LiF-BeF-ThF_4 (thermal gradient quenching and DTA cooling), LiF-BeF_2-UF_4 (DTA

Table 5.4: **Invariant equilibria in the ternary subsystems A-B-C of LiF-BeF_2-ThF_4-UF_4, calculated and *experimental (in italics)*[a]**

A	B	C	T/K	type invariant	phases present
LiF	BeF_2	ThF_4			
0.70	0.24	0.06	758.9	eutectic[b]	LiF + 3LiF·ThF_4 + 2LiF·BeF_2 = L
0.65	0.29	0.06	754.7	peritectic	3LiF·ThF_4 + LiF·ThF_4 + 2LiF·BeF_2 + L[c]
0.48	0.515	0.005	695.0	eutectic	2LiF·BeF_2 + BeF_2 + LiF·ThF_4 = L
0.34	0.65	0.01	751.0	peritectic	LiF·ThF_4 + LiF·2ThF_4 + BeF_2 + L[d]
0.66	*0.30*	*0.04*	*717*	*peritectic*	*LiF + 3LiF·ThF_4 + 2LiF·BeF_2 + L*
0.63	*0.30*	*0.07*	*721*	*peritectic*	*3LiF·ThF_4 + LiF·ThF_4 + LiF·2ThF_4 + L*
0.61	*0.36*	*0.03*	*706*	*peritectic*	*3LiF·ThF_4 + LiF·2ThF_4 + 2LiF·BeF_2 + L*
0.47	*0.51*	*0.02*	*629*	*eutectic*	*2LiF·BeF_2 + BeF_2 + LiF·2ThF_4 + L*
0.34	*0.64*	*0.03*	*728*	*peritectic*	*LiF·2ThF_4 + LiF·4ThF_4 + BeF_2 + L*
0.15	*0.83*	*0.02*	*770*	*peritectic*[f]	*ThF_4 +LiF·4ThF_4 + BeF_2 + L*
LiF	BeF_2	UF_4			
0.72	0.05	0.23	742.3		decomposition of 4LiF·UF_4
0.70	0.12	0.18	712.9	eutectic	LiF + LiF·UF_4 + 2LiF·BeF_2 = L
0.49	0.50	0.01	695.0	eutectic	2LiF·BeF_2 + LiF·UF_4 + BeF_2 = L
0.48	0.51	0.01	691.9	peritectic	2LiF·BeF_2 + LiF·4UF_4 + BeF_2 + L[e]
0.72	*0.06*	*0.22*	*753*	*peritectic*	*decomposition of 4LiF·UF_4*
0.69	*0.23*	*0.08*	*699*	*eutectic*	*LiF + LiF·UF_4 + 2LiF·BeF_2 + L*
0.48	*0.515*	*0.005*	*623*	*eutectic*	*2LiF·BeF_2 + LiF·UF_4 + LiF·4UF_4 + L*
0.455	*0.54*	*0.005*	*654*	*peritectic*	*2LiF·BeF_2 + LiF·4UF_4 + BeF_2 + L*
0.295	*0.70*	*0.005*	*756*	*peritectic*[f]	*UF_4 + LiF·4UF_4 + BeF_2 + L*
LiF	ThF_4	UF_4			
0.74	0.07	0.19	767.7	peritectic	LiF + LiF·(Th,U)F_4 + L[g]
0.735	0.015	0.25	760.2	eutectic	LiF + 4LiF·UF_4 + LiF·(Th,U)F_4 = L
0.56	0.10	0.34	903.8	peritectic	LiF·(Th,U)F_4 + LiF·4(Th,U)F_4 + L[h]
0.725	*0.07*	*0.205*	*773*	*peritectic*	*LiF + 3LiF·ThF_4 + 4LiF·UF_4*
0.72	*0.015*	*0.265*	*761*	*eutectic*	*LiF + 4LiF·UF_4 + LiF·(Th,U)F_4 + L*
0.63	*0.18*	*0.19*	*882*	*peritectic*	*LiF·(Th,U)F_4 + LiF·2ThF_4 + LiF·4(Th,U)F_4 + L*

[a] Values in *italics* are proposed values, based on experiments and extrapolation. LiF-BeF_2-ThF_4 was analyzed by Thoma *et al.* [78], LiF-BeF_2-UF_4 by Jones *et al.* [79] and LiF-ThF_4-UF_4 by Weaver *et al.* [80].

[b] 2LiF·BeF_2 was considered as incongruently melting compound at the time of analysis. However, detailed measurements by Romberger et al. [40] showed that it melts congruently, so that the peritectic can now be interpreted as eutectic point.

[c] Saddle point: 3LiF·ThF_4 + LiF·ThF_4 + 2LiF·BeF_2 + L = 2LiF·BeF_2 + L

[d] Saddle point: LiF·ThF_4 + LiF·2ThF_4 + BeF_2 + L = L

[e] Saddle point: 2LiF·BeF_2 + LiF·4UF_4 + BeF_2 = 2LiF·BeF_2 + L

[f] This peritectic point has not been found in the calculated diagram.

[g] Saddle point: LiF + LiF·(Th,U)F_4 + L = L

[h] Saddle point: LiF·(Th,U)F_4 + LiF·4(Th,U)F_4 + L = L

cooling, thermal gradient quenching and high-temperature filtration) and LiF-ThF_4-UF_4 (thermal gradient quenching). A comparison was made between liquidus surface of the calculated and the experimentally defined diagrams. Therefore, all liquidus data were carefully extracted from the data tables. Then the precipitation temperature of these compositions were calculated using the Equilib module in FactSage. The difference between model and experimental temperature was normalized by the experimental temperature T_{exp} and plotted versus T_{exp}. The results are shown in Figure 5. It can be seen that the agreement in all three systems is generally good, all within ± 10 %, while 79.1 % of the data agree better than ± 5 %. It must be noted, however, that the difference between the quenching and the cooling results is significant. A comparison was made between liquidus temperatures obtained by cooling and quenching for similar compositions. It appeared that differences from 20, 30, even up to 70 K are common. Thus, as the data scatter internally to this extent, it makes it complicated to determine the differences between the model and experiment. Performing our own DTA experiments would be priority in a future study on this system.

The asymmetric component in LiF-BeF_2-ThF_4

In an initial calculation of the LiF-BeF_2-ThF_4 diagram, it was assumed that BeF_2 was the chemically asymmetric component, which was given therefore a different weight in the Kohler-Toop extrapolation of the binary excess Gibbs coefficients. BeF_2 was selected because it is known to form polymeric species in the liquid phase and it was therefore anticipated to exert a different behavior than the other two compounds. This resulted in a ternary diagram with a significant miscibility gap in the BeF_2 corner, which is shown in Figure 5.10.

However, we realized after comparing the excess Gibbs energy curves of the three binaries that selecting LiF would be a better option.

As it can be seen in Figure 5.11, the excess Gibbs curves of LiF-BeF_2 and LiF-ThF_4 at 1100 K are both negative and of the same order of magnitude. This is in contrast to the BeF_2-ThF_4 curve, which is smaller and positive at the same temperature. This difference due to the presence of LiF could be explained by the fact that LiF is highly ionic, whereas BeF_2 and ThF_4 have the tendency to form more molecular-type ions as BeF_4^{2-} [83] and ThF_6^{2-} in the melt. Raman spectroscopy on molten LiF-BeF-ThF_4 mixtures could provide welcome information on the structure of the melt, because the model used

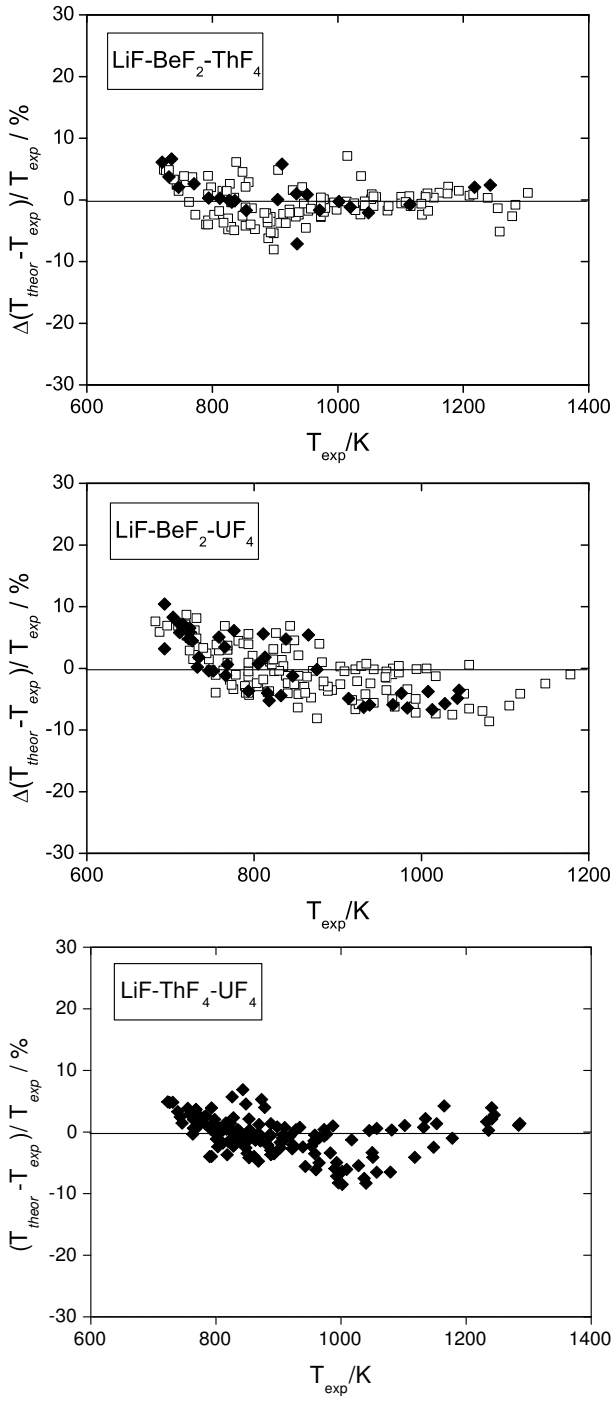

Figure 5.9: The difference between the calculated and the experimental ternary liquidus temperature T_{exp} of LiF-BeF_2-ThF_4, LiF-BeF_2-UF_4 and LiF-ThF_4-UF_4, normalized by T_{exp}, versus T_{exp}. Open symbols: obtained by cooling; closed symbols: obtained by quenching.

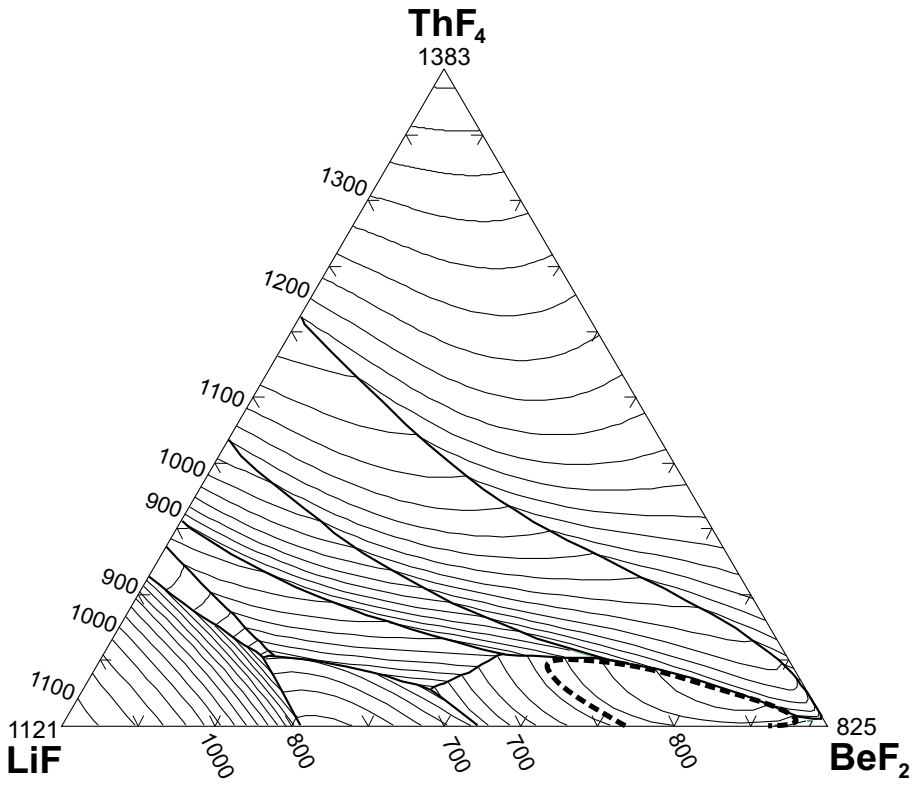

Figure 5.10: The calculated liquidus surface of LiF-BeF_2-ThF_4. The miscibility gap is indicated as a dashed line. Isotherms are labeled in K.

here is not conclusive.

The shape of the diagram, calculated by the LiF asymmetry model, resembles the experimental diagram from Thoma *et al.* [78] much better than the BeF_2 asymmetry model and also the overall agreement with the experimental data is better. However, there is a feature when comparing the two models, that should be noted. Concerning the LiF asymmetry model, the lowest temperatures appear to have the largest deviation from the experimental values, which can be seen in Figure 5, where the disagreement is slightly increasing with decreasing temperatures. This inevitably holds that the ternary invariant points, which belong to the lowest temperatures in the system, differ more from the experimental data than the liquidus at higher temperatures. A check was performed on the temperature dependance of the excess Gibbs energy. Therefore, a number of extra terms were introduced in the excess Gibbs energy function to see whether a better description could be obtained at the lower temperatures, but without satisfying result.

A similar plot comparing the model with the experiments was made for BeF_2 asymmetry as well. In this case, the deviations from the experimental data are larger and more scattered through the temperature spectrum. So, here it could happen that the invariant temperatures showed a better agreement with the experiments [82], but the compositions deviated more.

The miscibility gap present in LiF-BeF_2 has its influence on the ternaries LiF-BeF_2-ThF_4 and LiF-BeF_2-UF_4, where a small gap can be found close to the LiF-BeF_2 axis. However, the addition of exactly 1.0 mole % of ThF_4 and 0.9 mole % UF_4, which was revealed by systematically calculated pseudobinary diagrams crossing the ternary demixing areas, is enough to suppress this two-phase field. Hence it is explicable that Thoma *et al.* [78] and Jones *et al.* [79] do not mention the existence of ternary miscibility gaps.

Next to the miscibility gap, a couple of minor differences were found in the comparison with the invariant points of LiF-BeF_2-ThF_4, see Table 5.4, due to a change in the field stability of $LiThF_5$. Thoma *et al.* proposed the $LiF{\cdot}ThF_4$ phase to be stable in a small part of the diagram, ending in a peritectic at 0.63 LiF-0.30 BeF_2-0.07 ThF_4. In our model, this field is broader and ends in the peritectic at 0.34 LiF-0.65 BeF_2-0.01 ThF_4. A possible explanation could be the fact that four intermediate LiF-ThF_4 compounds exist of which we do not have thermodynamic data. They were optimized in the binary system, but it cannot be excluded that the description of the thermodynamic parameters is not sufficient for extrapolation in a ternary system.

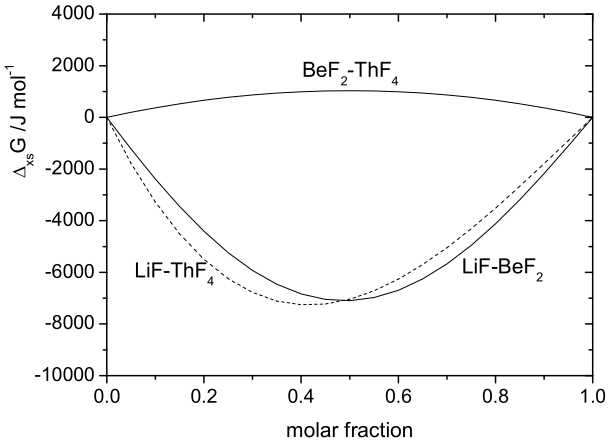

Figure 5.11: The excess Gibbs energy curves of LiF-BeF_2, LiF-ThF_4 (dashed line) and BeF_2-ThF_4.

Cross-section through LiF-BeF_2-ThF_4

Figure 5.12 is an example of a cross-section through the LiF-BeF_2-ThF_4 diagram. It shows the complexity of the system, especially below the liquidus. It can be seen that the model reproduces the available liquidus data well, with the exception of the range $0.3 < X_{BeF_2} < 0.4$. Here the ORNL data show even an increase towards the eutectic, whereas the model decreases in temperature. Something else that should be noted is the number of observed thermal effects that exceeds the number of phase boundaries. It can be partly explained by the fact that one intermediate compound, $LiBeF_3$, has deliberately been omitted from the assessment, since it decomposes in the solid phase and has no influence on the liquidus. But otherwise, it is interesting to have a closer examination of the range $0.2 < X_{BeF_2} < 0.4$ and to repeat the ORNL experiments to have more certainty which thermal signal corresponds to which phase transition. Generally, it would be helpful to know the intensity of the observed effects. We know from previous DTA measurements [24], that the formation of a eutectic or peritectic melt gives the largest signal, much more than when the liquidus is crossed. One can wonder if the two observed liquidus signals at X_{BeF_2}=0.221, T=754.9 K and X_{BeF_2}=0.244, T=758.5 K are probably not misinterpreted eutectic and peritectic events? They coincide namely almost exactly with our calculated ternary invariant points of 758.9 K and 754.7 K,

see Table 5.4.

In general, it can be concluded that the polynomial model with Kohler-Toop extrapolation gives a satisfactory description of the binary and the higher order systems of LiF-BeF_2-ThF_4-UF_4, especially LiF-BeF_2-UF_4, LiF-ThF_4-UF_4 and BeF_2-ThF_4-UF_4, since the diagrams agree with the determined invariant points and the experimental liquidus data. Nevertheless, it might be worthwhile for a future study to use another model, for example the quasi-chemical model in quadruplet approximation by Pelton *et al.* [53], to see if the agreement with experiments and model can be improved. For the system LiF-NaF-LaF_3 we made already a comparison between the results obtained by the quadruplet model and by the polynomial description we used in this study. In that case it appeared that the differences are minor, but it is not certain what the results will be in LiF-BeF_2-ThF_4-UF_4.

Comparison quaternary model and experimental data

A comparison considering the possible composition for a Molten Salt Reactor was also made. The Molten Salt Breeder Reactor, MSBR, was designed in the 1960's to breed ^{233}U from ^{232}Th in a LiF-BeF_2 melt. A favorable composition was 71.7 % LiF- 16 % BeF_2- 12 % ThF_4- 0.3 % UF_4 in moles, with the small amount of UF_4 to start the reaction [4]. The temperature of fusion was determined to be 773 ± 5 K, according to a report by Cantor [49]. This is in reasonable agreement with the somewhat higher calculated temperature of 794.5 K, which is the precipitation temperature of the composition 71.7 % LiF- 16 % BeF_2- 12.3 % $(Th_{0.9756}U_{0.0244})F_4$. It has been found as well that without the addition of 0.3 % UF_4 the precipitation temperature would increase by exactly 2 K. Four possible compositions for breeder fuel, which were analyzed by Cantor [49], appear in Table 5.5 with the experimentally determined and calculated temperatures.

The vapor pressure of MSR Breeder fuel

Low vapor pressures at the operating temperature are desirable for safety reasons. The partial vapor pressures of the gaseous phase were calculated in the temperature range 400-1500 K for the typical Molten Salt Breeder fuel,

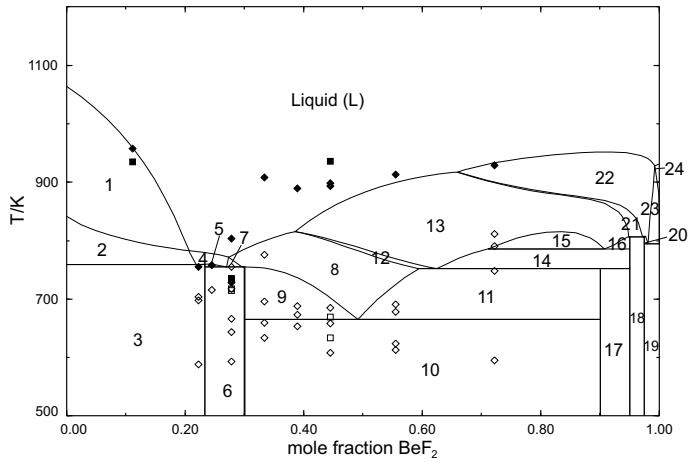

Figure 5.12: Pseudobinary $Li_{0.9}Th_{0.1}F_{1.3}$ - $Be_{0.9}Th_{0.1}F_{2.2}$ section of the pseudoternary LiF-BeF_2-ThF_4 system. ■ liquid, obtained by quenching; ♦ liquid, obtained by cooling; □ other phase transitions obtained by quenching; ◊ other thermal effects occurring on cooling, all data extracted from tables according to Thoma et al. [78]. Phases: 1 LiF+L; 2 LiF+Li_3ThF_7+L; 3 LiF+Li_3ThF_7+Li_2BeF_4; 4 Li_3ThF_7+L; 5 Li_3ThF_7+Li_2BeF_4+L; 6 Li_2BeF_4+Li_3ThF_7+$LiThF_5$; 7 Li_3ThF_7+$LiThF_5$+L; 8 $LiThF_5$+L; 9 Li_2BeF_4+$LiThF_5$+L; 10 Li_2BeF_4+$LiThF_5$+BeF_2; 11 $LiThF_5$+BeF_2+L; 12 $LiThF_5$+$LiTh_2F_9$+L; 13 $LiTh_2F_9$+L; 14 $LiTh_2F_9$+BeF_2+L; 15 $LiTh_2F_9$+L+L_2; 16 $LiTh_2F_9$+L; 17 $LiThF_5$+$LiTh_2F_9$+BeF_2; 18 $LiTh_2F_9$+$LiTh_4F_{17}$+BeF_2; 19 $LiTh_4F_{17}$+ThF_4+BeF_2; 20 $LiTh_4F_{17}$+BeF_2+L; 21 $LiTh_2F_9$+$LiTh_4F_{17}$+L; 22 $LiTh_4F_{17}$+L, 23 $LiTh_4F_{17}$+ThF_4+L; 24 ThF_4+L

Table 5.5: **Compositions of MSR Breeder fuel as proposed by ORNL with experimental and calculated temperature**

LiF	BeF_2	ThF_4	UF_4	T_{exp}/K	T_{cal}/K
0.73	0.16	0.107	0.003	773	790
0.72	0.21	0.067	0.003	773	794
0.68	0.20	0.117	0.003	753	785
0.63	0.25	0.117	0.003	773	790

as mentioned in the *Thermodynamic assessment* section. The calculations were performed using the Equilib module in the FactSage software package. $\Delta_f H^0$(298.15 K), S^0(298.15 K) and C_p for the gaseous phase for every component present in the vapor were needed to calculate the partial and the total vapor pressures. The values were extracted from the NIST-JANAF thermochemical tables [29] and are listed in Table 5.6. For the liquid phase the solution model as presented in the *Thermodynamic assessment* section was used.

Figure 5.13 shows the partial and total vapor pressures of the Molten Salt Breeder fuel composition. LiF also exists as a dimer, Li_2F_2, in the gas. It can be seen that over the whole temperature range the total vapor pressure is dictated by BeF_2. In the range 750-900 K, in which the MSR will operate, the total pressure increases from 10^{-8} to 10^{-6} bar. This is a low value and it proves that this fluoride mixture meets the demand of a low vapor pressure in a MSR system at working temperatures.

Cantor *et al.* [49] investigated the vapor pressure of MSBR fuel. He proposed a pressure-temperature relation according to Eq. 5.1. This function is also plotted in Figure 5.13 and it can be seen that the agreement between the calculated and the experimental values is good.

$$^{10}\log(p/\text{torr}) = 8.0 - \frac{10000}{T/\text{K}} \tag{5.1}$$

Eq. 5.1 was estimated from the vapor pressure measurements of LiF-BeF_2 mixtures by Cantor *et al.* [84]. Compared were the mixtures with the same LiF/BeF_2 ratio as in MSBR fuel, which is 81.8 mole % LiF to 18.2 mole % BeF_2. At T = 1273 K, $^{10}\log(p/\text{bar})$ is -2.48 and at T = 1373 K $^{10}\log(p/\text{bar})$

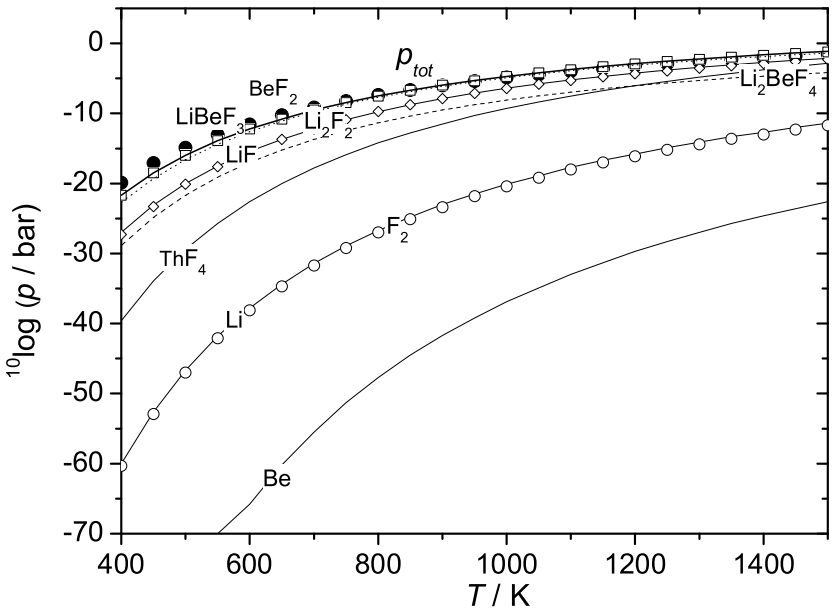

Figure 5.13: The partial and total vapor pressures of a typical Molten Salt Breeder fuel composition. Plotted as well is the total vapor pressure (•) as given by Cantor *et al.* [49].

Table 5.6: $\Delta_f H^0(298.15\ \mathbf{K})/\mathbf{kJ{\cdot}mol^{-1}}$, $S^0(298.15\ \mathbf{K})/\mathbf{J{\cdot}K^{-1}{\cdot}mol^{-1}}$ **and** C_p **data for the components in the gas phase with composition 0.717 LiF - 0.16** $\mathbf{BeF_2}$ **- 0.123** $\mathbf{ThF_4}$

X	$\Delta_f H^0$	S^0	a	bT /K	cT^2 /K^2	dT^3 /K^3	eT^{-2} /K^{-2}
LiF	-340.575	200.28	32.31	$7.513{\cdot}10^{-3}$	$-3.249{\cdot}10^{-6}$	$5.010{\cdot}10^{-10}$	$-2.657{\cdot}10^{5}$
Li_2F_2	-942.781	258.63	79.21	$3.470{\cdot}10^{-3}$	$-7.641{\cdot}10^{-7}$		$-1.515{\cdot}10^{6}$
$LiBeF_3$	-1390.30	292.58	113.2	$2.995{\cdot}10^{-3}$	$2.701{\cdot}10^{-6}$	$5.008{\cdot}10^{-10}$	$-1.144{\cdot}10^{4}$[b]
Li_2BeF_4	-1958.20	324.45	173.4	$-3.112{\cdot}10^{-3}$	$-1.001{\cdot}10^{-6}$	$3.217{\cdot}10^{-10}$	$-1.979{\cdot}10^{4}$[b]
BeF_2	-796.190	227.56	47.30	$1.895{\cdot}10^{-2}$	$-8.438{\cdot}10^{-6}$	$1.259{\cdot}10^{-9}$	$-5.216{\cdot}10^{5}$
ThF_4[a]	-1748.20	351.56	122.4	$-1.406{\cdot}10^{-2}$	$7.365{\cdot}10^{-6}$	$-1.939{\cdot}10^{-9}$	$-7.545{\cdot}10^{3}$[b]

[a] An extra term appeared to fit the C_p function optimally: $2.011{\cdot}10^{-13}T^4/\mathrm{K}^4$.

[b] This coefficient is eT^{-1}/K^{-1}.

is -1.93. The calculated total vapor pressure $^{10}\log(p_{cal}/\mathrm{bar})$ for LiF-BeF_2 at the same conditions was -2.43, respectively -1.75, which is in good agreement with the experimental values.

The density of MSR Breeder fuel

The density of mixtures

Engineers need to know the density of the fuel mixture for the reactor design. Densities of pure components are usually known, but data on the densities of mixtures are scarcer. In this section it is investigated how the density of mixtures can be derived from the density of the pure components.

The density ρ is defined as the ratio of the molar weight M and the molar volume V_m:

$$\rho/\mathrm{kg}\cdot\mathrm{m}^{-3} = \frac{M/10^3\ \mathrm{g}\cdot\mathrm{mol}^{-1}}{V_m/\mathrm{m}^3} \tag{5.2}$$

The molar weight of a mixture is simply the sum of the molar weights of its components:

$$\mathrm{M} = \sum N_i M_i \tag{5.3}$$

For the molar volume this is only the case for ideal mixtures:

$$\mathrm{V}_{idm} = \sum N_i V_i \tag{5.4}$$

resulting in a linear variation as a function of composition in case of a binary system. In practise many mixtures are not ideal but real, and deviations from the linearity can be observed:

$$\mathrm{V}_m = V_{idm} + V_{exs} \tag{5.5}$$

It should be noted that the melting point of a mixture is often much lower than that of the end member compounds, and the measurements for the mixture are made in a temperature range where the liquid phases of the end member compounds are thermodynamically not stable. In that case the experimental molar volume of the end-member compounds is extrapolated to the supercooled state.

LiF-BeF_2

The density of liquid LiF-BeF_2 has been measured by Blanke *et al.* [85] from 0 mole % to 55 mole % BeF_2, and Cantor *et al.* [86] for 50.2, 74.9 and 89.2 mole % BeF_2. The results are shown in Figure 5.14 in an isothermal section for T = 1073 K of the molar volume. This figure confirms the linear dependence on the mole fraction and thus the additivity of the molar volumes. It can also be seen that the result of Cantor [87] is in perfect agreement with the relation based on the experimental molar volume of BeF_2 and the extrapolated molar volume of LiF in the supercooled state.

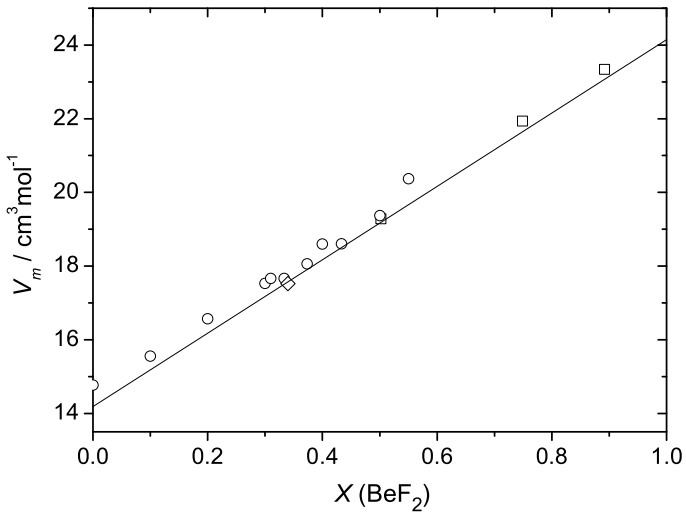

Figure 5.14: The molar volume of liquid LiF-BeF_2 at 1073 K; ∘ Blanke *et al.* [85], □ Cantor *et al.* [86]; ♢ Cantor [87]; the line represents V_m of the ideal mixture.

LiF-ThF$_4$

The density of LiF-ThF$_4$ mixtures was measured by Porter and Meaker [88] and Hill *et al.* [89]. The results are in good agreement and clearly indicate a linear dependence of the molar volume with composition, confirming ideal behavior, which is shown in Figure 5.15.

BeF$_2$-ThF$_4$

The density of liquid BeF$_2$-ThF$_4$ has not been determined experimentally. However, the density of the liquid of the analogous system BeF$_2$-UF$_4$ was measured by Blanke *et al.* [85], though only for a single composition (35 mol% UF$_4$). The molar volume derived from this value (30.4 cm$^3\cdot$ mol^{-1} at T = 1073 K) is in reasonable agreement with the value calculated for an ideal mixture of the pure components (31.9 cm$^3\cdot$ mol^{-1}), taking into account the uncertainties for the value for BeF$_2$.

LiF-BeF$_2$-ThF$_4$

Since the molar volumes of the liquid phases of the LiF-BeF$_2$ and LiF-ThF$_4$ binaries show ideal behavior, the same can be assumed for the LiF-BeF$_2$-ThF$_4$ ternary system. The densities in the ternary can thus be simply calculated from the molar volume and the molar weight.

The density of LiF-BeF$_2$-ThF$_4$ of three compositions with almost constant LiF concentration was measured by Cantor [87]. As shown in Table 5.7, the molar volumes derived from these data are in excellent agreement with those calculated from the pure components.

Viscosity of LiF-BeF$_2$-ThF$_4$

As density, viscosity is also a key parameter for reactor design. Data on the pure components are known, but data on the viscosity of mixtures are scarcer. In this section we investigate ways to estimate the viscosity of a ternary mixture.

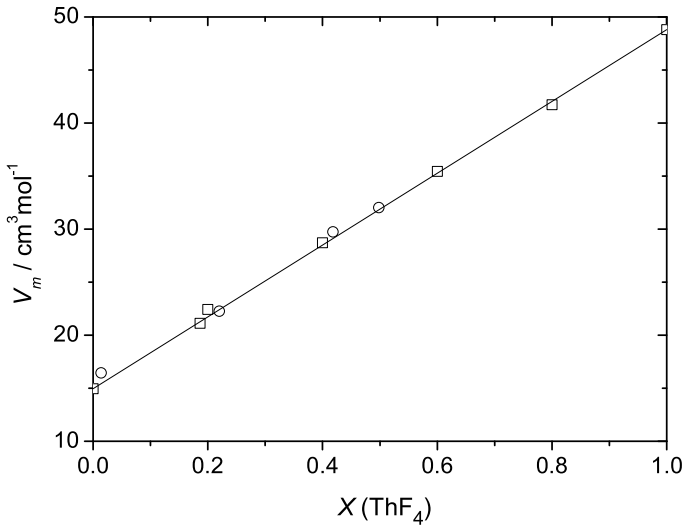

Figure 5.15: The molar volume of liquid LiF-ThF_4 at 1273 K; ∘ Porter and Meaker [88], □ Hill *et al.* [89]; the line represents V_m of the ideal mixture.

Table 5.7: **The molar volumes of three LiF-BeF_2-ThF_4 mixtures at T = 1073 K: the experimental data from Cantor [87] and the calculated values from the end-members.**

X LiF	X BeF_2	X ThF_4	$V_{m,exp}$/cm^3· mol^{-1}	$V_{m,cal}$/cm^3· mol^{-1}
0.7011	0.2388	0.0601	20.0	20.0
0.7006	0.1796	0.1198	21.4	21.6
0.6998	0.1499	0.1503	22.4	22.4

The dynamic viscosity of a melt can be related to the Gibbs energy of activation for viscous flow, ΔG^*, by Eq. 5.6.

$$\eta = \frac{\mathrm{Nh}\rho}{M}\exp\left(\frac{\Delta G^*}{\mathrm{R}T}\right) \tag{5.6}$$

where ρ is the density of the melt in kg·m^{-3}, h is Planck's constant, N is Avogadro's number, M is molecular weight in g·mol^{-1}, T is the absolute temperature in K and R is the universal gas constant. Seetharaman *et al.* [90] proposed a method to estimate the viscosity of ternary silicate melts by suggesting that ΔG^* is the sum of the ideal activation energy for viscous flow and the thermodynamic excess Gibbs energy of mixing. We attempted to follow his method for our ternary fluoride system. However, when applying this method to the fluorides, we did not find a good result using the thermodynamical excess Gibbs energy of mixing.

We suggest that the viscosity of a ternary system can be described in a similar way as the thermodynamic properties of the liquid phase in a ternary diagram. Analogously to the thermodynamic Gibbs energy of mixing in a solution phase, which exists of a sum of the Gibbs energy of the pure components and a mixing term, the viscosity can be described as the sum of the activation energy of the pure components (the ideal part) plus an extra term that covers the ideal and the excess mixing part of the activation energy in a multicomponent system, as in Eq. 5.7.

$$\Delta G^* = \Delta_{\mathrm{id}} G^* + \Delta_{\mathrm{ex}} G \tag{5.7}$$

Data on the viscosity of LiF-BeF$_2$ [86, 91] and LiF-ThF$_4$ [92], which are plotted in Figure 5.16, respectively Figure 5.17, were used to derive the excess activation energy terms. For each composition, the viscosity η was given, such that every η is valid for a certain temperature range. By η, defined in Eq. 5.6, the total ΔG^* is known and its T-dependance can be fitted as a first order polynomial '$a + bT$'. So for every composition and temperature, ΔG^* can be calculated. The weighted average of ΔG^* for the pure components is the ideal term $\sum_i X_i\ \Delta G_i^*$. The extra term in the Gibbs energy of activation for LiF-BeF$_2$ and LiF-ThF$_4$, calculated as the total ΔG^* subtracted by the ideal part, can be described as the Redlich-Kister polynomials in Eq. 5.8, respectively Eq. 5.9. $\Delta_{\mathrm{ex}} G$ is plotted for LiF-BeF$_2$ and LiF-ThF$_4$ in Figure 5.18.

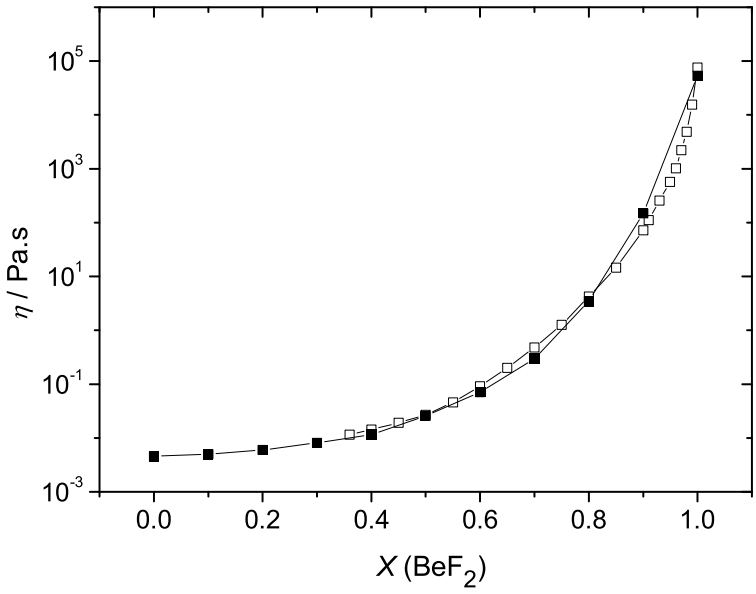

Figure 5.16: The dynamic viscosity of LiF-BeF_2 at 873 K by Cantor *et al.* [86] (□) and Desyatnik *et al.* [91] (■).

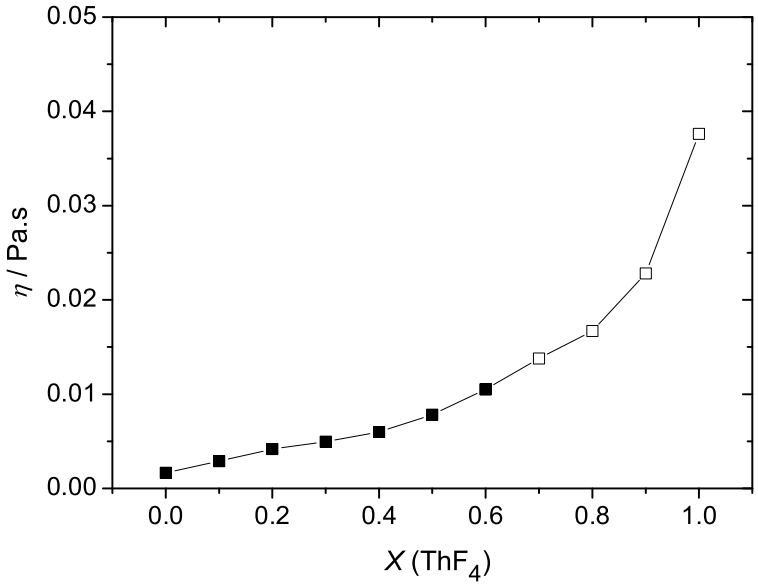

Figure 5.17: The dynamic viscosity of LiF-ThF$_4$ at 1200 K by Chervinskii *et al.* [92]. Open symbols indicate the extrapolation of the viscosity function in the supercooled region.

$$\Delta_{\mathrm{ex}}G^{*}_{LiF-BeF_2} = X_{BeF_2}X_{LiF}\ (-284015 \cdot X_{BeF_2} * -57618 \cdot X_{LiF}) \qquad (5.8)$$

$$\Delta_{\mathrm{ex}}G^{*}_{LiF-ThF_4} = X_{ThF_4}X_{LiF}\ (-22110 \cdot X_{ThF_4} * +17081 \cdot X_{LiF}) \qquad (5.9)$$

The viscosity of BeF_2-ThF_4 is not known. However, we treat the system LiF-BeF_2-ThF_4 as a binary system with xLiF - (1-x)BeF_2 as one and xLiF - (1-x)ThF_4 as the other end-member. Basically, the system is reduced as the sum of pseudobinary systems BeF_2-ThF_4 with a constant molar fraction of LiF. Eqs. 5.8 and 5.9 are substituted in Eq. 5.7 to calculate the activation energy for viscous flow. It should be noted that calculating the ternary viscosity by this way was analogous to the calculation of ternary phase diagrams from the binaries, where one would speak of an asymmetrical extrapolation, with LiF as the asymmetric component, exactly as was done for the LiF-BeF_2-ThF_4 diagram. By using Eq. 5.6, the viscosity of LiF isopleths in LiF-BeF_2-ThF_4 could be calculated. Plotted in Figure 5.19 is the viscosity for BeF_2-ThF_4 at a constant molar fraction of LiF = 0.70, since this is approximately the fraction of LiF in MSBR fuel.

A few data are available for the viscosity in LiF-BeF_2-ThF_4. One data point was reported by MacPherson [93] and three by Cantor *et al.* [49] for X_{LiF} = 0.70. It can be seen that the calculated viscosity follows the trend of the experimental data well. Also the values of model and data are in agreement, considering the uncertainty range of 25 % for the experimental data indicated by Cantor.

However, concise conclusions cannot be drawn from the comparison with four data points. More data are needed to study the viscosity model used here in more detail. To complete the model, we would need viscosity measurements on the binary BeF_2-ThF_4 system and more viscosity data on the ternary system would be desirable as well.

Conclusion on Molten Salt Breeder Fuels

The phase behavior, vapor pressure, density and viscosity of the candidate system for Molten Salt Breeder fuel, LiF-BeF_2-ThF_4 have been calculated. A

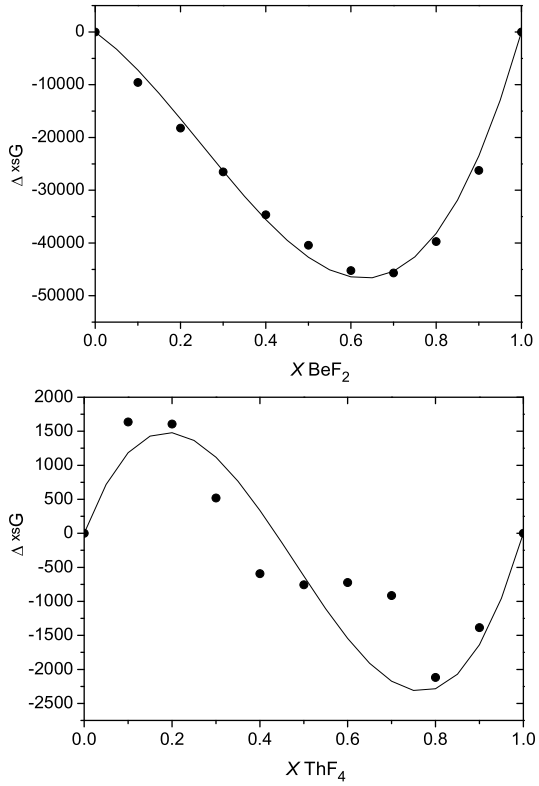

Figure 5.18: The excess activation energy for viscous flow for LiF-BeF_2 and LiF-ThF_4, fitted with a Redlich-Kister polynomial.

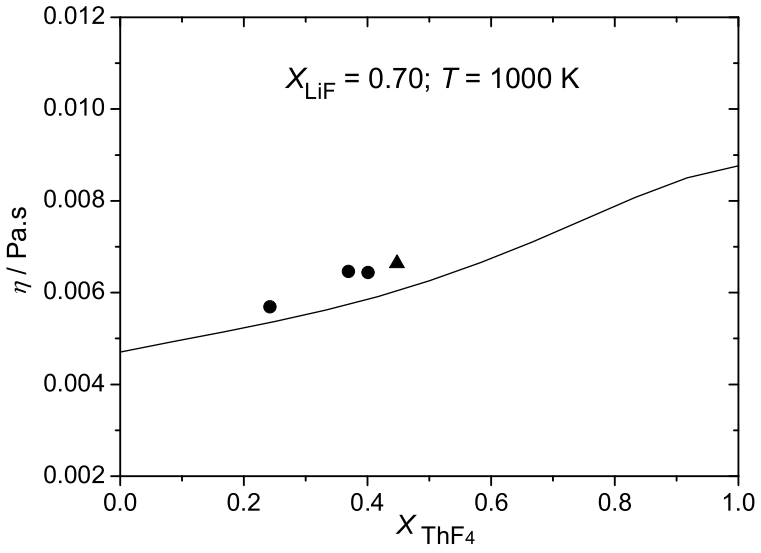

Figure 5.19: The pseudobinary ThF_4-BeF_2 viscosity diagram at 1000 K; at a constant molar fraction of LiF = 0.70. ▲ MacPherson [93]; • Cantor *et al.* [49].

typical composition is 0.717 LiF - 0.16 BeF_2 - 0.12 ThF_4 - 0.003 UF_4, which is in this case simplified to 0.717 LiF - 0.16 BeF_2 - 0.123 ThF_4. The temperature of fusion, according to our calculated phase diagram, is 794.5 K, which is in agreement, but slightly higher than the 773 ± 5 K, reported by Cantor [49].

The vapor pressure of this composition at the operating temperature of a MSR (750-900 K) is low, namely between 10^{-8} and 10^{-6} bar. It is fully dictated by the partial vapor pressure of BeF_2.

A linear relationship exists between the density of the pure molten fluoride components and the density of a liquid mixture. The density of MSR fuel could therefore be calculated as the weighted average from the densities of liquid LiF, BeF_2 and ThF_4. The calculated and the experimental values were in perfect agreement: 21.6, respectively 21.4 $cm^3 \cdot mol^{-1}$.

The dynamic viscosity of a molten fluoride mixture can be calculated from the activation energy for viscous flow. This consists, analogously to the thermodynamic Gibbs energy of mixing, of an ideal and an excess part. The excess activation energy was derived from the viscosity data on LiF-BeF_2 and LiF-ThF_4 and was described as Redlich-Kister polynomials. The viscosity of LiF-BeF_2-ThF_4 at a constant molar fraction of LiF = 0.70 was calculated and compared to the few data available. It appeared that the values and the trend of the model and data were in agreement. The calculated viscosity of MSBR fuel is $6.0 \cdot 10^{-3}$ Pa·s to $6.6 \cdot 10^{-3}$ Pa·s reported by ORNL researchers. However, the number of data are too scarce to draw conclusions. More data on binary and ternary systems are needed for a better understanding of viscous flow in molten fluorides.